ORIGINAL PAPER

Silicone phantoms fabricated with multi-material extrusion 3D printing technology mimicking imaging properties of soft tissues in CT

Sepideh Hatamikia [a,b,*], Laszlo Jaksa [a], Gernot Kronreif [a], Wolfgang Birkfellner [c], Joachim Kettenbach [d], Martin Buschmann [e], Andrea Lorenz [a]

[a] Austrian Center for Medical Innovation and Technology (ACMIT), Wiener Neustadt, Austria
[b] Research Center for Medical Image Analysis and Artificial Intelligence (MIAAI), Department of Medicine, Danube Private University, Krems, Austria
[c] Center for Medical Physics and Biomedical Engineering, Medical University of Vienna, Vienna, Austria
[d] Institute of Diagnostic, Interventional Radiology and Nuclear Medicine, Landesklinikum Wiener Neustadt, Wiener Neustadt, Austria
[e] Department of Radiation Oncology, Medical University of Vienna/AKH Wien, Vienna, Austria

Received 30 December 2022; accepted 21 May 2023

Abstract

Recently, 3D printing has been widely used to fabricate medical imaging phantoms. So far, various rigid 3D printable materials have been investigated for their radiological properties and efficiency in imaging phantom fabrication. However, flexible, soft tissue materials are also needed for imaging phantoms for simulating several clinical scenarios where anatomical deformations is important. Recently, various additive manufacturing technologies have been used to produce anatomical models based on extrusion techniques that allow the fabrication of soft tissue materials. To date, there is no systematic study in the literature investigating the radiological properties of silicone rubber materials/fluids for imaging phantoms fabricated directly by extrusion using 3D printing techniques. The aim of this study was to investigate the radiological properties of 3D printed phantoms made of silicone in CT imaging. To achieve this goal, the radiodensity as described as Hounsfield Units (HUs) of several samples composed of three different silicone printing materials were evaluated by changing the infill density to adjust their radiological properties. A comparison of HU values with a Gammex Tissue Characterization Phantom was performed. In addition, a reproducibility analysis was performed by creating several replicas for specific infill densities. A scaled down anatomical model derived from an abdominal CT was also fabricated and the resulting HU values were evaluated. For the three different silicone materials, a spectrum ranging from −639 to +780 HU was obtained on CT at a scan setting of 120 kVp. In addition, using different infill densities, the printed materials were able to achieve a similar radiodensity range as obtained in different tissue-equivalent inserts in the Gammex phantom (238 HU to −673 HU). The reproducibility results showed good agreement between the HU values of the replicas compared to the original samples, confirming the reproducibility of the printed materials. A good agreement was observed between the HU target values in abdominal CT and the HU values of the 3D-printed anatomical phantom in all tissues.

Keywords: 3D printing; Silicone materials; Radiological properties; CT imaging

* Corresponding author. Sepideh Hatamikia, Austrian Center for Medical Innovation and Technology, Wiener Neustadt, Austria.
E-mail: sepideh.hatamikia@acmit.at (S. Hatamikia).

Z Med Phys **xxx** (2023) xxx–xxx
https://doi.org/10.1016/j.zemedi.2023.05.007
www.elsevier.com/locate/zemedi

1 Introduction

Additive manufacturing (AM), also known as three-dimensional (3D)-printing, is increasingly used to fabricate complex structures from physical models generated from three-dimensional (3D) computer-aided design (CAD) data [1]. Recently, 3D-printing has also become popular for the development of medical imaging phantoms [2-4]. The material used in such imaging phantoms should ideally mimic physical and imaging characteristics as close as possible to human tissue [5,6]. The radiological properties of any tissue equivalent material can be characterized by Hounsfield Unit (HU) which represents linear attenuation coefficient of X-rays in CT [7]. Solid materials such as Polymethyl methacrylate (PMMA) and resins [8-10] have been proposed to mimic soft tissues HUs for a breathing thorax and pelvis CT phantoms. In addition, several rigid 3D printable materials have been examined regarding to their radiological properties, e.g. Acrylonitrile butadiene styrene (ABS), Polylactic acid (PLA), Polyamid 12 (Nylon12 or PA12), Acrylonitrile styrene acrylate (ASA Pro), Polyethylenterephthalat (PETG), Vero PureWhite and VeroClear [3,11-13] and different infill density (ratio of printing material and air) were used to adjust different CT contrasts [10-12]. for these However, flexible soft tissue materials are needed for imaging phantoms used for different scenarios where anatomical deformations should be simulated, for example motion-adaptive radiotherapy treatments [14,15], phantoms with respiratory motion for needle based liver interventions [16] and phantoms for different needle-based surgery training [17-19].

Several studies have proposed deformable imaging phantoms. Various types of non-printable flexible materials were investigated with the goal of soft-tissue phantom constructions, e.g. gelatin, silicone and urethane materials. Gelatin materials have shown similar radiological properties to soft tissue [20,21]. However, the drawback of such gelatin-based phantoms is that the radiological properties usually change over time, as they are losing water. Synthetic polymers, for example polyvinyl chloride (PVC) and silicone have generally more stable properties and also a longer shelf life because they do not have water within the structure [22]. It was also shown that PVC with different softener ratios can result in different HU, allowing the replication of many organ densities [21,23,24]. Furthermore, silicone and urethane materials have been used to study soft tissues, with different types and mixtures providing the ability to adjust concentrations to mimic the relevant HU [2,14,21,25]. Although the aforementioned flexible materials [2,20-25] showed similar radiological properties to soft tissues and organs, they are mainly used to fill phantoms developed using molding techniques, so direct 3D printing of deformable phantoms was not possible.

In medical imaging, 3D printing technology is now being explored for directly creating phantoms from flexible, 3D-printable tissue-like materials. While 3D-printing with thermoplastic filaments – also called fused deposition modeling (FDM) – is a widely accessible technology, it is limited in printing soft rubbers [3]. However, printing with soft rubbers – like silicones – is beneficial in anatomic models where mechanical realism is important. Such rubber models can be directly printed by extruding liquid rubber with a suitable extruder. In a previous study, 3D-printable rubber-elastomeric polymer called PORO-LAY filaments were used to develop tissue mimicking materials for MRI phantoms [26]. In this case, an FDM printer with dual extruders was used for printing. In another study [27] radiological characteristics of PORO-LAY filament materials were investigated by measuring their HU values at different infill structures, infill densities and introduction of several kinds of fluids into the infill structures. Such objects printed with porous filaments (like PORO-LAY) first need to be soaked in water for multiple days to achieve their final properties.[1,2] In comparison, 3D-printable silicone rubbers cure upon deposition and reach their final mechanical properties in some time after curing, without needing further post-processing. Moreover, one cannot achieve a hardness lower than approx. Shore A 40 with porous filaments.[1,2] One further option to produce soft 3D-printed objects with an extrusion-based process is the use of various filaments loaded with thermoplastic polyurethane (TPU). These materials do not require post-processing after printing, but they are even more limited in hardness, with non-foaming versions having a Shore A hardness above approx. 90, and foaming versions staying above approx. Shore A 60.[3] In contrast, silicone rubbers can be significantly softer, with some 3D-printable silicones going as low as Shore A 5 in hardness.[4,5]

Different silicone additive manufacturing technologies have been used to fabricate anatomical models based on extrusion processes [28-32]. These include the fabrication of tissue-like aortic heart valves by combining spray and extrusion processes [29], the fabrication of standard molded silicone coupons as well as silicone meniscus implants using a custom 3D silicone printer and two-part Ecoflex silicone resins [30,31] and the printing of various objects and

[1] www.orbi-tech.de/shop/3D-Filamente/Poro-Lay:::72_125.html
[2] www.matterhackers.com/store/3d-printer-filament/poro-lay-lay-fomm-filament-175mm[3] https://colorfabb.com/varioshore-tpu-natural
[3] https://colorfabb.com/varioshore-tpu-natural
[4] www.cop-chimie.com/en/product-category/3d-printing/
[5] www.elkem.com/markets/advanced-manufacturing-industrial/molding-printing/3d-printing-additive-manufacturing/

Please cite this article as: S. Hatamikia, L. Jaksa, G. Kronreif et al., Silicone phantoms fabricated with multi-material extrusion 3D printing technology mimicking imaging properties of soft tissues in CT, Z Med Phys, https://doi.org/10.1016/j.zemedi.2023.05.007

anatomical models using a multi-material 3D extrusion printer capable of printing 1k silicone and an additional viscous fluid, combined with a standard filament print head [33,34]. However, in the above studies [28-34], radiological properties of the 3D printed silicone materials were not investigated.

The use of 3D-printed silicone materials in imaging phantoms can be very beneficial for scenarios where flexibility and softness of materials is important [14-18,27,29-32]. In addition, the influence of different infill densities (ratio of material to air) on the resulting radiodensity in CT imaging using different filament materials has been extensively studied [12,27,35], but no such study has been reported for printable silicon materials. Therefore, the aim of this study was to evaluate the radiological properties of extrusion silicone 3D printed phantoms in CT imaging. The HU values of three different 3D printed silicone materials as well as their tunability to mimic different soft tissues by varying the printed infill density were analyzed. In addition, the reproducibility of the method was checked and a comparison with the Gammex Tissue Characterization Phantom was performed. Furthermore, a first anatomical phantom is presented, mimicking realistic radiodensity of a human abdominal CT slice.

2 Materials and methods

2.1 Silicone 3D printing

In the current study, a custom-built silicone 3D-printer (Railcore Labs LIC.), based on a commercially available Railcore II 300 ZL filament printer was used (Fig. 1). The moving carriage of this base printer was extended with a Viscotec Vipro-HEAD 3/3 (Viscotec GmbH, Töging am Inn, DE) fluid printhead, which consists of two independently controllable extruders. This way, the printhead can deposit either two high-viscosity fluids independently, or alternatively a two-component material. Further details about this 3D-printer are found in [33,34]. In this study, three single-component (1k) condensation-crosslinking liquid silicone rubbers (supplied by Elkem Silicones SAS, Lyon, France) were used with 0.41 mm nozzles on the fluid extruders. The individual print runs were planned in the open-source slicing software PrusaSlicer v2.3.0. The silicone printhead was calibrated according to calibration method described in [34].

2.2 3D printed samples

To explore the connection between infill structure density and radiological properties, several rectangular blocks (called samples in this study) of $14 \times 14 \times 20$ mm were printed from the three silicone rubber materials, namely Elkem AMSil 20101 (Material 1), 20102 (Material 2) and 20103 (Material 3). The various infill structure densities covered a range of 30% to 100% material volume fraction, with 10% increments between 30% and 60%, 5% increments between 65% and 75%, and 3% increments between 79 and 100% yielding 15 levels in total. The corresponding samples are called S1-S15 accordingly, with S1 belonging to 100% infill and S15 to 30% infill (Fig. 2). The 100% infill test phantom was printed with a rectilinear infill structure, while all the other samples were printed with a gyroid infill structure generated in PrusaSlicer software (Fig. 2). The samples were printed in batches of approximately 7–10 samples in a single print run. The levels of 40%, 70% and 91% were printed 6 times of each material to evaluate reproducibility, while all other levels were printed once of each material. All samples were printed with a 20 mm/s printing speed, two solid closing layers on top and bottom, two contour lines on the sides (solid shell), in ambient conditions of 20–30 °C and 65–85% relative humidity. The samples were

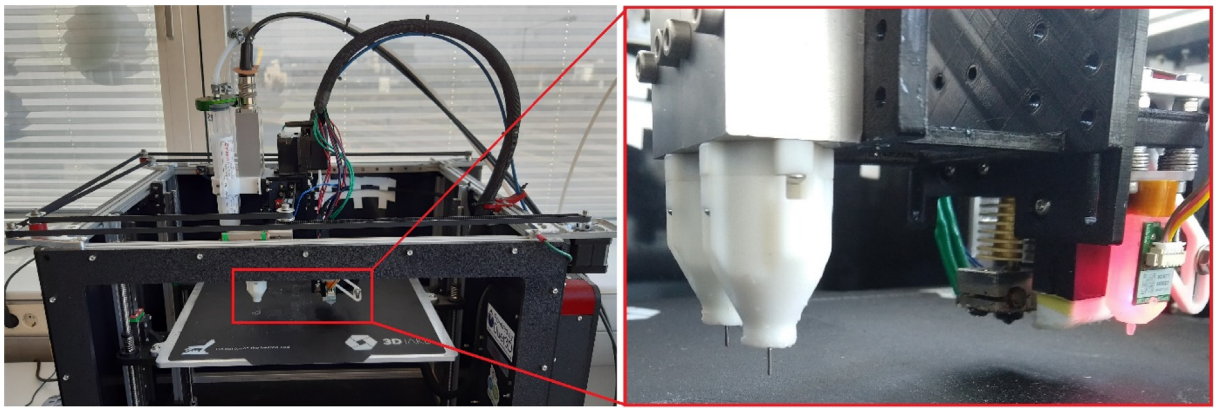

Figure 1. (Left image) the multi-material printer used in this study. (Right image) both independently controllable fluid extruders are shown.

Please cite this article as: S. Hatamikia, L. Jaksa, G. Kronreif et al., Silicone phantoms fabricated with multi-material extrusion 3D printing technology mimicking imaging properties of soft tissues in CT, Z Med Phys, https://doi.org/10.1016/j.zemedi.2023.05.007

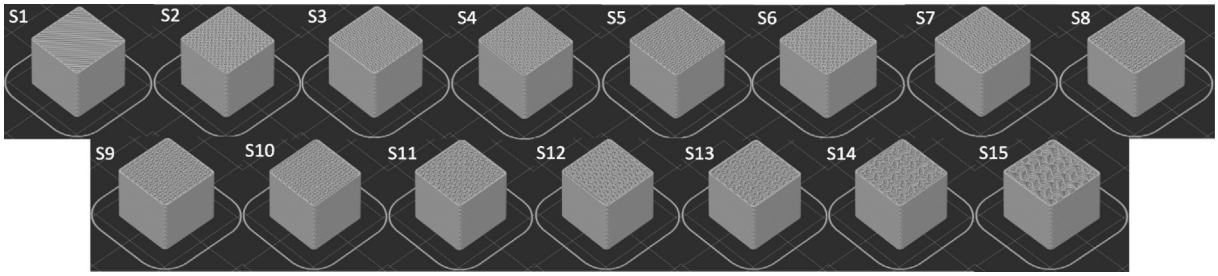

Figure 2. The gyroid infill structures generated in PrusaSlicer software for different infills including S1-S15 corresponding to 100% to 30% material volume fraction, with 10% increments between 30% and 60%, 5% increments between 65% and 75%, and 3% increments between 79 and 100%.

removed from the building platform 24 hours after printing to allow sufficient crosslinking. PrusaSlicer estimates the weight of an object to be printed based on the given material mass density, and the material volume needed to print all the required trajectories to form the desired object. Assessing the accuracy of this estimation was not in the scope of this study.

2.3 HU analysis

All the samples as well as the anatomical phantom were scanned with the standard clinical CT protocol (SOMATOM Definition AS, Siemens Healthineers, Erlangen Germany, tube current time product 70 mAs for samples and 150 mAs for anatomical phantom, tube voltage 120 kVp, slice thickness 0.60 mm, pixel spacing 0.77 mm, reconstruction kernel J30s) and the resulted radiodensities were computed. Additional scans at 100 kVp and 80 kVp were also performed from all phantoms in order to report the resulting HU at different energy spectra. In case of the anatomical phantom the obtained HU values were compared with those of the original human CT data. Analyze 12.0 toolkit (AnalyzeDirect, Over-land Park, United States) was used in order to measure the HU value from the samples CT scans using similar approach as in previous studies [11,12,35,38-40]. Different line profiles inside some regions of interests within the phantom images were selected and the HU values were computed by calculating the average and the standard deviation over all points for the selections related to those line profiles. In addition, for each test phantom. Signal-to-noise-ratio (SNR) was also calculated by dividing the achieved average of HU values to the standard deviation of HU values, the absolute values were reported.

2.4 Comparison with standard Gammex tissue equivalent phantom

The resulting HU values from the developed samples were compared with a standard phantom, the Gammex Tissue Characterization Phantom (Gammex Model 467, Middleton, USA). A CT scan from the standard Gammex phantom was obtained with the same CT parameters (only at 120 kVp) as for 3D printed samples (Section 2.3). The average and standard deviation (SD) of the resulting HU related to the Gammex tissue equivalent inserted cylinders including bone mineral, inner bone, liver, brain, solid water, breast, adipose and lung were calculated using Analyze 12.0 toolkit with the same method as in Section 2.3. The relation between different tissue equivalent inserted cylinders and the printed samples with different ratios was also investigated.

2.5 Mass density measurement

The nominal density for Material 1, Material 2 and Material 3 according to their technical data sheets are 1.01 g/cm^3, 1.30 g/cm^3 and 1.04 g/cm^3, respectively. We calculated the mass density of the printed samples based on measured weight and estimated volume from PrusaSlicer. The samples were weighed on a KERN EMB 200-3 laboratory scale (Kern&Sohn GmbH, Balingen, Germany). The measured weight was compared to the nominal weight estimations of PrusaSlicer to ensure that all printed specimens fall within a relative weight error range of ±5%. The estimated weight of the internal structure was calculated as the total measured weight of a given phantom minus the estimated weight of just the (empty) solid shell based on PrusaSlicer, which was different for all three materials due to the different material densities. The estimated volume of the internal structure was calculated as the nominal total volume of the phantom shape (approx. 3.903 cm^3 for all samples) based on PrusaSlicer, minus the estimated volume of just the (empty) solid shell based on PrusaSlicer (approx. 0.638 cm^3 for all phantoms of all materials). These were used to calculate the mass density of the internal structure of the phantoms, because the HU results are only based on this internal gyroid structure, not the solid shell of a given phantom. The mass density of the internal structures (excluding the solid shell) of all 3D-printed samples was then calculated by dividing the estimated weight (in g) of the internal structure by the estimated volume of the internal structure.

Please cite this article as: S. Hatamikia, L. Jaksa, G. Kronreif et al., Silicone phantoms fabricated with multi-material extrusion 3D printing technology mimicking imaging properties of soft tissues in CT, Z Med Phys, https://doi.org/10.1016/j.zemedi.2023.05.007

2.6 Reproducibility of the silicone samples

A reproducibility analysis was also performed to ensure the reproducibility of the radiation density of the proposed phantoms. For this aim, different infill density levels (replicas) of each material were printed (Section 2.2) to evaluate reproducibility. The replicas were scanned using the same CT parameters as for the 3D printed samples (Section 2.3) and also HU values (in terms of average and standard deviation) were calculated with the same HU analysis as described in Section 2.3.

2.7 Anatomical phantom

As a first use case of the HU/infill density mapping acquired through examining the samples, a radiological phantom representing a simplified scaled down anatomical model derived from an abdominal CT [11] was printed using the Material 1 (translucent) and 20102 (white) silicones. The CT data were anonymized (the available information includes slice thickness 3 mm, pixel spacing 0.7 mm, exposure time = 6644 ms). It was processed in order to obtain 3D data using 3D Slicer software 4.11.2 (Boston, MA, USA). Major anatomic structures were roughly segmented using the region-growing algorithm, distinguishing the bone, kidney and vessels, liver and spleen, muscle, connective tissue as well as the air in lungs and abdomen (Fig. 3). The approximate HU values within these structures were 759, 175, 96, 32, −65, and −794, respectively. One slice of the torso was selected from this dataset and within this slice, segmentation was manually refined. The segments were smoothened and exported in STL format.

The exported segments were post-processed in Autodesk Meshmixer v3.5 (Autodesk Inc., San Francisco, CA) to correct smaller meshing errors. Afterwards, they were reassembled in PrusaSlicer (Fig. 3). According to the approximate HU values determined for each tissue, the corresponding air/material ratios were introduced as a gyroid infill volume fraction to each segment, based on the prior radiodensity analysis of the samples (described in 2.2). The resulting radiological phantom slice was printed with a 45% layer-plane scaling and a 7.5 mm thickness. Both halves of the fluid printhead were used, one loaded with Material 2 to print the bone segments and the other with Material 1 to print all other segments with their corresponding gyroid infill densities. The first and last (or bottom and top) layer of the phantom had a 100% rectilinear infill for all the segments. The phantom also had a single solid contour line surrounding its edge across all layers. These measures were taken to make the phantom more robust overall, and to reduce the risk of damage during detachment from the building platform and transport. However, the individual segments inside the phantom were not separated by any solid contour, to improve realism in CT. The resulted anatomical phantom underwent CT scan (similar imaging parameters as in Section 2.3 only for 120 kVp) and the average and standard deviation over different segmentation was also computed using similar approach as introduced in Section 2.3 (one example of employed line profiles (Section 2.3) within each segmentation area is shown in Fig. 3B). HU values the obtained HU values were compared with those of the original human CT data.

3 Results

3.1 3D printed samples results

The three materials printed with different infill densities S1-S15 (Section 2.2) were printed successfully (Fig. 4) and a CT scan was acquired (Fig. 5). The average HUs for the scan with 120 kVp were calculated (Table 1), yielding a range between −639 to 252 HUs, −485 to 770 HUs and −612 to 316 for Material 1, Material 2 and Material 3, respectively. The HU for samples printed with Materials 1 and 3 were lower than for samples of Material 2. For decreasing X-ray energy (100kVp and 80kVp), an increase in HU was observed (Fig. 6).

3.2 Comparison of the resulting HU with the Gammex phantom

The axial slice of the CT scan of the Gammex phantom is shown in Fig. 5. HU values for different tissue equivalent inserts inside the Gammex phantom including bone mineral, inner bone, liver, brain, solid water, breast, adipose and lung were calculated using the same method as described in Section 2.3 (Table 2). For all three printed materials, the closest achieved HU to the Gammex phantom inserts and the corresponding infill density is reported in Table 3. According to the results, the samples could achieve similar radiodensity range as achieved in the Gammex phantom including 238 HU to −673 HU (bone mineral to lung) when using different infill densities. In addition, lower standard deviation and higher absolute value of SNR was observed in the samples compared to the different tissue equivalent inserts inside the Gammex phantom.

3.3 Resulting mass densities of samples

The mass density values (g/cm^3) (Section 2.5) were calculated for all 3D printed samples at different infill densities (Table 3). The relation between the mass density and HU of the samples (at 120 kV) with respect to different infill densities for material 2 is also shown (Fig. 7). Both mass density and HU values showed an almost similar trend of increasing values when increasing infill density.

Please cite this article as: S. Hatamikia, L. Jaksa, G. Kronreif et al., Silicone phantoms fabricated with multi-material extrusion 3D printing technology mimicking imaging properties of soft tissues in CT, Z Med Phys, https://doi.org/10.1016/j.zemedi.2023.05.007

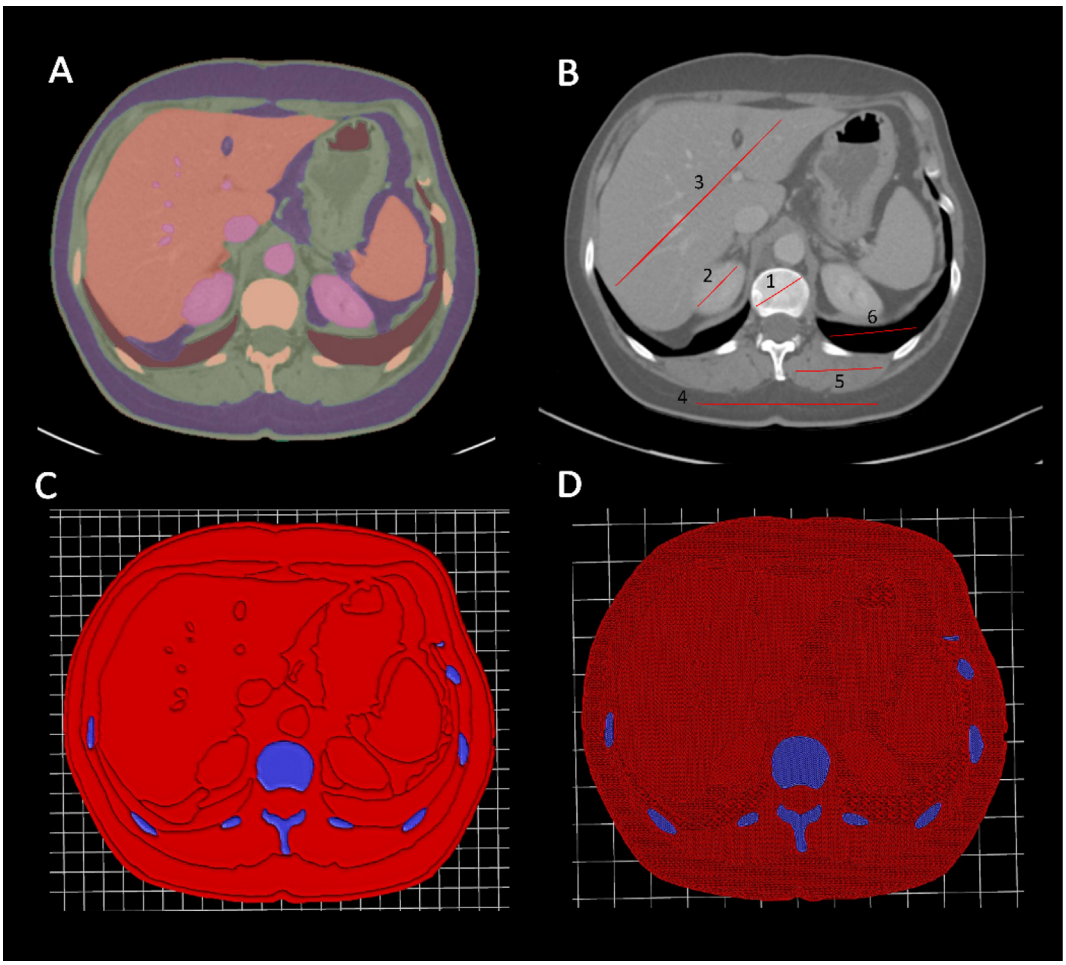

Figure 3. (A), (B): Segmented abdominal slice and one example of the selected line profile for HU analysis, separating the (1) bone (yellow), (2) kidney and vessels (pink), (3) liver and spleen (orange), (4) connective tissue (purple), (5) muscle, skin and abdomen (green) as well as the (6) air in the lungs and abdomen (brown). The segments were reassembled in Prusa Slicer (C) and their corresponding gyroid infill percent was assigned to them (D). The red and blue structures in (C) and (D) are printed with Material 1 and Material 2, respectively. Note: several line profiles within each region were selected and the standard deviation over all points for the selections related to those line profiles were calculated for each region, but we only visualize one line profile per region in (B) for simplicity).

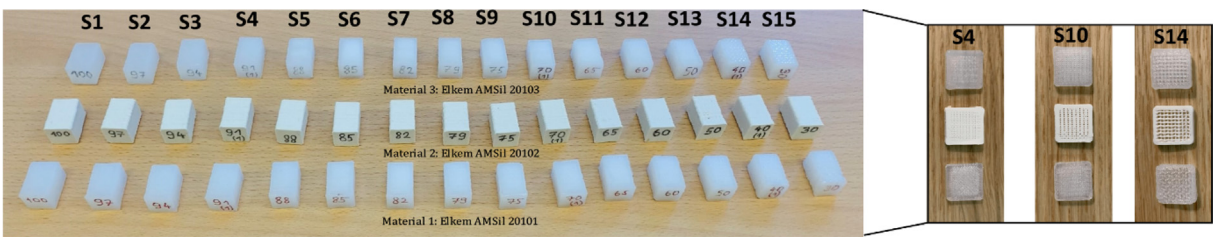

Figure 4. The 3D printed samples related to the three printed materials (down: Material 1, middle: Material 2, up: Material 3) at different infill densities (S1-S15) and the corresponding cross sections at S4, S10 and S14.

Please cite this article as: S. Hatamikia, L. Jaksa, G. Kronreif et al., Silicone phantoms fabricated with multi-material extrusion 3D printing technology mimicking imaging properties of soft tissues in CT, Z Med Phys, https://doi.org/10.1016/j.zemedi.2023.05.007

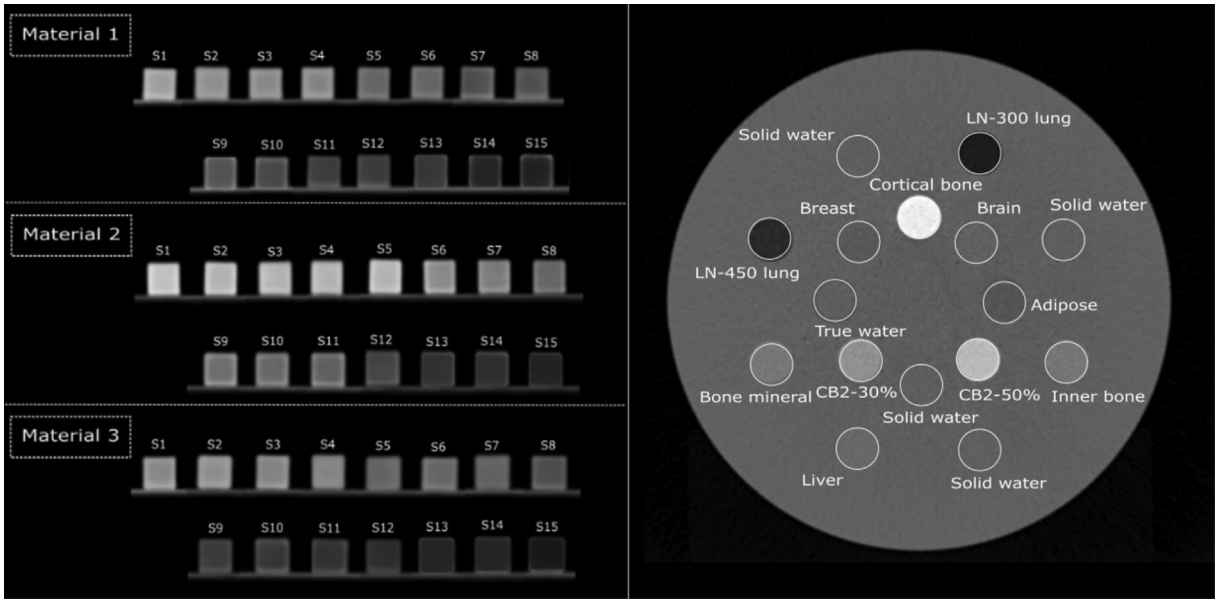

Figure 5. (Left): The axial view of the CT scan at 120 kV from all samples related to Material1, Material 2 and Material 3 at different infill densities S1-S15. (Right): Axial slice of the CT scan of the Gammex phantom including different tissue equivalent inserts. The display window shows linear attenuation coefficient and is set to the range [-270–1900].

Table 1
Hounsfield Unit (HU) and standard deviation (SD) and signal-to-noise (SNR) ratio related all three materials at different infill densities at 120 kV.

Infill density (%)	Material 1			Material 2			Material 3		
	HU	SD	SNR	HU	SD	SNR	HU	SD	SNR
100 (S1)	252	1.87	135	771	2.66	290	316	1.05	301
97 (S2)	196	2.47	79	699	2.77	252	313	1.13	277
94 (S3)	158	2.61	61	591	2.74	216	291	2.03	143
91 (S4)	158	2.91	54	586	3.33	176	212	2.26	94
88 (S5)	142	3.02	44	604	3.24	186	202	3.65	55
85 (S6)	45	3.30	14	500	3.20	227	70	2.20	32
82 (S7)	27	1.86	14	505	3.95	128	59	2.64	22
79 (S8)	12	2.11	2	441	3.17	139	30	2.19	14
75 (S9)	−40	2.21	18	357	2.54	141	19	2.01	10
70 (S10)	−153	1.82	84	202	1.95	104	−95	1.29	74
65 (S11)	−212	1.52	140	68	1.86	37	−207	1.50	138
60 (S12)	−223	1.49	150	00	2.05	00	−198	1.46	136
50 (S13)	−354	1.66	213	−166	2.14	78	−354	1.65	214
40 (S14)	−499	1.68	297	−298	2.13	140	−496	1.68	295
30 (S15)	−639	2.06	310	−485	2.56	190	−612	2.16	284

3.4 Resulting radiodensity for the replicas

The average HU and standard deviation over the CT scan from the 6 replicas related to the three materials at 40%, 70% and 91% infill densities were calculated (Table 4). The mean HU values found over the replicas for all materials and infill densities revealed a good reproduction of the original densities (Table 1).

3.5 3D printed anatomical phantom results

The anatomical phantom was printed successfully (Fig. 8A). According to the HU values achieved in Section 3.1, we assigned the materials and the infill densities which corresponded to the organs/tissues radiodensity for the anatomical phantom (Table 5). The axial slice of the resulting CT scan from the anatomical phantom is shown

Please cite this article as: S. Hatamikia, L. Jaksa, G. Kronreif et al., Silicone phantoms fabricated with multi-material extrusion 3D printing technology mimicking imaging properties of soft tissues in CT, Z Med Phys, https://doi.org/10.1016/j.zemedi.2023.05.007

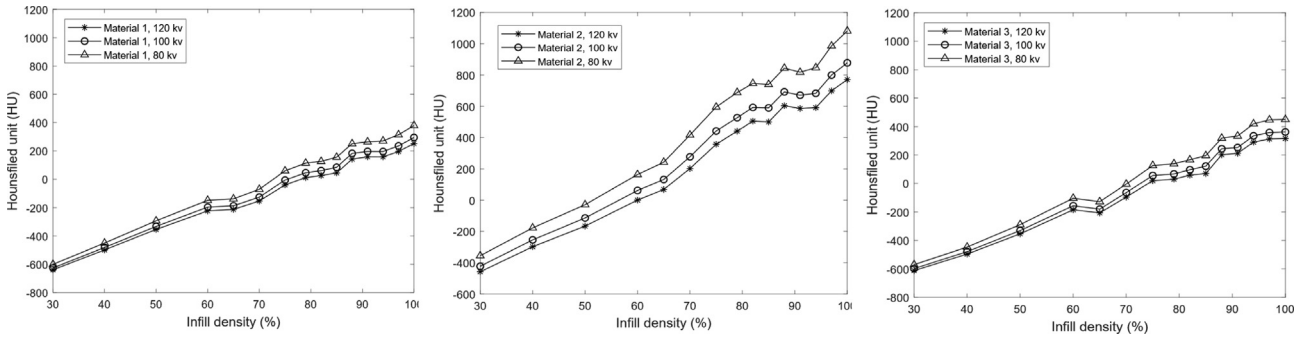

Figure 6. Resulting HU values for three materials for the three different scan settings including 120 kVp, 100 kVp and 80 kVp.

Table 2
Table showing the mean Hounsfield Unit (HU) at 120 kV, standard deviation (SD) and signal-to-noise ratio (SNR) of the resulting HU related to the Gammex tissue equivalent inserted cylinders including bone mineral, inner bone, liver, brain, solid water, breast, adipose and lung and the corresponding materials and infill densities with the closest HUs from the printed samples. Mat.1: Material 1, Mat.2: Material 2, Mat.3: Material 3.

Gammex phantom	HU+SD, SNR	Printed Material (Infill density (%))	HU+SD, SNR
Bone mineral	238 ± 17, 14	Mat.1 (100)	252 ± 1.87, 135
		Mat.2 (70)	202 ± 1.95, 104
		Mat.3 (91)	212 ± 2.26, 94
Inner bone	210 ± 12, 18	Mat.1 (97)	196 ± 2.47, 79
		Mat.2 (70)	202 ± 1.95, 157
		Mat.3 (88)	202 ± 3.65, 55
Liver	66 ± 10, 7	Mat.1 (85)	45 ± 3.30, 14
		Mat.2 (65)	68 ± 1.86, 37
		Mat.3 (82)	59 ± 2.64, 22
Brain	25 ± 6, 4	Mat.1 (82)	27 ± 1.86, 14
		Mat.2 (60)	0 ± 2.05, 00
		Mat.3 (79)	30 ± 2.19, 14
Solid Water	−1 ± 3, 0	Mat.1 (79)	12 ± 2.11, 3
		Mat.2 (60)	0 ± 2.05, 0
		Mat.3 (75)	19 ± 2.01, 10
Breast	−72 ± 10, 7	Mat.1 (75)	−40 ± 2.21, 18
		Mat.2 (60)	0 ± 2.05, 0
		Mat.3 (70)	−95 ± 1.29, 72
Adipose	−109 ± 13, 8	Mat.1 (70)	−153 ± 1.82, 84
		Mat.2 (50)	−166 ± 2.14, 78
		Mat.3 (70)	−95 ± 1.29, 72
Lung-450	−476 ± 12, 40	Mat.1 (40)	−499 ± 1.68, 297
		Mat.2 (30)	−485 ± 2.56, 190
		Mat.3 (40)	−496 ± 1.68, 295
Lung-300	−673 ± 15, 45	Mat.1 (30)	−639 ± 2.06, 310
		Mat.2 (30)	−485 ± 2.56, 190
		Mat.3 (30)	−613 ± 2.16, 284

in Fig. 8B and compared with patient CT (Fig. 8C). The resulting HU values were calculated (same method as in Section 2.3) from the CT scan from this phantom (Table 5). The approximate HU values within the phantom for corresponding structures of bone, kidney and vessels, liver and spleen, muscle, connective tissue and lung tissues (Fig. 3) were achieved 727, 151, 102, −17, −92, −680, respectively. With the exception of the lung, a good agreement was obtained between the target HU values (approximate HU values from abdominal CT) and the HU values of the fabricated phantom in all tissues of the phantom. The HU values related to different line profiles indicated in Fig. 3B for the

Please cite this article as: S. Hatamikia, L. Jaksa, G. Kronreif et al., Silicone phantoms fabricated with multi-material extrusion 3D printing technology mimicking imaging properties of soft tissues in CT, Z Med Phys, https://doi.org/10.1016/j.zemedi.2023.05.007

Table 3
Mass density values (g/cm^3) for all samples.

Infill density (%)	Material 1 (g/cm^3)	Material 2 (g/cm^3)	Material 3 (g/cm^3)
100% (S1)	1.050	1.389	1.084
97% (S2)	0.961	1.273	1.034
94% (S3)	0.966	1.202	0.995
91% (S4)	0.926	1.177	0.936
88% (S5)	0.919	1.190	0.935
85% (S6)	0.836	1.057	0.833
82% (S7)	0.821	1.104	0.857
79% (S8)	0.827	1.067	0.847
75% (S9)	0.785	1.003	0.835
70% (S10)	0.712	0.931	0.750
65% (S11)	0.670	0.818	0.717
60% (S12)	0.650	0.750	0.683
50% (S13)	0.552	0.642	0.556
40% (S14)	0.439	0.673	0.443
30% (S15)	0.325	0.570	0.350

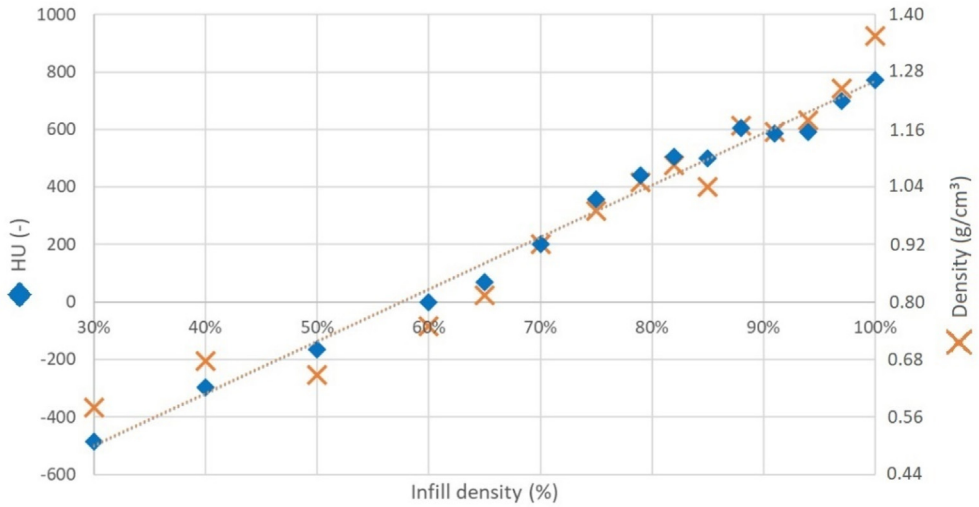

Figure 7. The relation between the mass density and HU of the samples (at 120 kV) with respect to different infill densities used for material 2.

patient CT compared to the fabricated anatomical phantom are shown in Fig. 9.

4 Discussion and conclusion

3D-printing technology is widely used in producing medical imaging phantoms. Anthropomorphic 3D printed imaging phantoms mimicking tissues and contrasts in real patients with regard to X-ray attenuation can be very valuable to produce phantoms for image quality optimization, comparison of image quality between different imaging systems, dosimetry, quality control and imaging protocol definition. In this study, the radiological properties of extrusion silicone 3D printed phantoms in CT imaging were investigated. The HU values of three different silicone printing materials at different infill densities were assessed in order to modify their radiological properties and to achieve a spectrum of radiodensity that mimics different soft tissues and organs. The 3D printed samples made of three different materials were able to produce a HU spectrum in the range of −639 to +780 HU in CT at a scan setting of 120 kVp, which corresponds not only to the radiation attenuation of human soft tissue, but also of bones and lungs. We also investigated the performance of our approach using an anatomical phantom (generated from a human abdominal CT) containing complex structures and combinations of

Please cite this article as: S. Hatamikia, L. Jaksa, G. Kronreif et al., Silicone phantoms fabricated with multi-material extrusion 3D printing technology mimicking imaging properties of soft tissues in CT, Z Med Phys, https://doi.org/10.1016/j.zemedi.2023.05.007

Table 4
The average HU and standard deviation over the CT scan from the 6 replicas related to the three materials at 40%, 70% and 91% infill densities.

	Infill density = 91 %			Infill density = 70 %			Infill density = 40 %		
	Mat.1 (HU)	**Mat.2 (HU)**	**Mat.3 (HU)**	**Mat.1 (HU)**	**Mat.2 (HU)**	**Mat.3 (HU)**	**Mat.1 (HU)**	**Mat.2 (HU)**	**Mat.3 (HU)**
Replica 1	158	586	212	−153	202	−95	−499	−298	−496
Replica 2	111	575	184	−127	228	−67	−502	−319	−498
Replica 3	158	539	184	−139	189	−85	−493	−318	−528
Replica 4	111	524	256	−166	237	−116	−495	−279	−491
Replica 5	162	559	169	−108	219	−101	−497	−291	−479
Replica 6	159	611	131	−175	226	−82	−491	−254	−476
Mean HU	143	566	189	−145	217	−91	−496	−293	−495
Standard deviation HU	25	32	42	25	18	17	4	25	18

different infill density structures and materials within the same phantom. We observed good agreement between the HU target values in the abdominal CT of the reference patient and the HU of the 3D printed anatomical phantom in all tissues (except for lung) confirming the successful replication of several contrasts in patient dataset using the multiple different infill densities. Printing materials with infill densities lower than 30% could lead to HU of the lungs, but this is accompanied by printing instability and collapse in the printed sample due to the high air content.

So far, several phantoms mimicking soft tissue radiodensities in CT imaging have been reported in the literature and their radiological properties were evaluated; however, these phantoms were mainly made of rigid materials [3,11-13]. Deformable 3D-printed imaging phantoms can be very beneficial for various scenarios [14-19]. Recently, different silicone additive manufacturing technologies have already been proposed to manufacture flexible and soft anatomical models based on extrusion techniques [28-34]. To our knowledge, there is no systematic study reported in the literature that explores the radiological properties of 3D direct printing of silicone materials/fluids for imaging phantoms manufactured using extrusion-based printer. Furthermore, the impact of different infill densities to adjust radiodensity in CT imaging on such printable silicon materials has not been investigated. Our study investigated the radiological properties of the 3D printed silicone phantoms directly printed based on extrusion technique. A good similarity was also observed between the radiodensity of the silicone samples and different tissue-equivalent Gammex phantom inserts. However, a further tuning of radiodensity values is also feasible by adjusting the HU values using smaller infill density steps, e.g., using step size of 1% for infill density. In total, lower standard deviation and higher absolute value of SNR was observed in the samples compared to the different tissue equivalent inserts inside the Gammex phantom. This suggests the efficiency of the 3D printed silicone materials in producing CT imaging phantoms. Reproducibility test results also showed a good agreement between the HU values of the replicas compared to the initial samples, confirming reproducibility of the printed materials. The mass density of all 3D printed samples was computed and evaluated at different infill densities. As can be seen from the results of Table 4, the samples with the infill densities that contained a higher percentage of air had lower density values, which was due to a lower weight.

A scaled down anatomical model derived from an abdominal CT was fabricated. Reducing printing time and material costs were two important considerations for reducing the size of the anatomical phantom in this study. However, we acknowledge the limitation imposed by the printer size. We downsized the phantom to 116.2 × 131.3 × 7.5 mm, but the maximum size of our

Please cite this article as: S. Hatamikia, L. Jaksa, G. Kronreif et al., Silicone phantoms fabricated with multi-material extrusion 3D printing technology mimicking imaging properties of soft tissues in CT, Z Med Phys, https://doi.org/10.1016/j.zemedi.2023.05.007

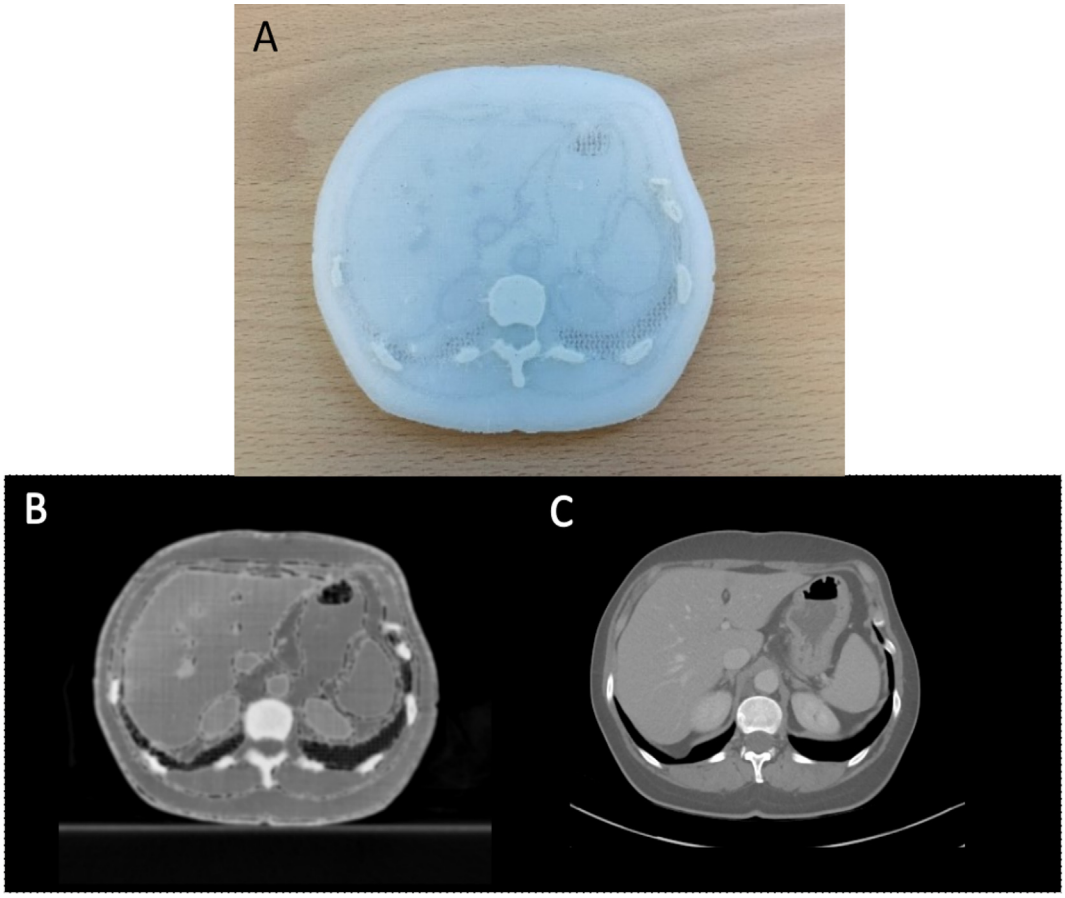

Figure 8. A) the 3D printed anatomical phantom, B) axial slice of the CT scan from the 3D printed anatomical phantom, C) axial slice of the abdominal CT scan. The phantom was printed with a 45% layer-plane scaling compared to real patient scan. The display window shows linear attenuation coefficient and is set to the range [-270–1600].

Table 5
The mean and standard deviation (SD) of the resulting HU at 120 kV of the anatomical phantom compared to target HU values (approximate HU from abdomen CT) as well as corresponding test phantom materials and infill densities used for different tissues.

Tissue type	Material, infill density	Patient HU	Anatomical phantom HU
Bone	Mat 2, 100%	759 ± 54.12	727 ± 3.27
Kidney and vessels	Mat 1, 97%	175 ± 34.31	151 ± 2.78
Liver and spleen	Mat 1, 88%	96 ± 30.56	102 ± 4.28
Muscle	Mat 1, 82 %	32 ± 27.52	−17 ± 3.35
Connective tissue	Mat 1, 75 %	−65 ± 38.46	−92 ± 4.15
Lung	Mat 1, 30%	−794 ± 29.84	−680 ± 3.18

printer that can be printed at one time is higher (200 × 250 × 250 mm), so printing a larger phantom was feasible, but it was not possible to print the entire patient-sized phantom at once. We would like to mention that we can print in parts and glue them together (similar to our previous work [35]) if a real anatomy size phantom is the goal, but that was not the focus of this study. The main reason to print an anatomical phantom here was to show whether the idea of contrast matching to achieve target contrasts can be applied to the anatomical phantom.

Some non-linearity could be observed in increasing HU (and also the measured mass density) when increasing infill densities (e.g., for HU values related to infill densities of 82–94% for material 2 (Table 1 and Fig. 8)). Concerning the accuracy of the infill structure generation and printing process, certain limitations may have influenced the density

Please cite this article as: S. Hatamikia, L. Jaksa, G. Kronreif et al., Silicone phantoms fabricated with multi-material extrusion 3D printing technology mimicking imaging properties of soft tissues in CT, Z Med Phys, https://doi.org/10.1016/j.zemedi.2023.05.007

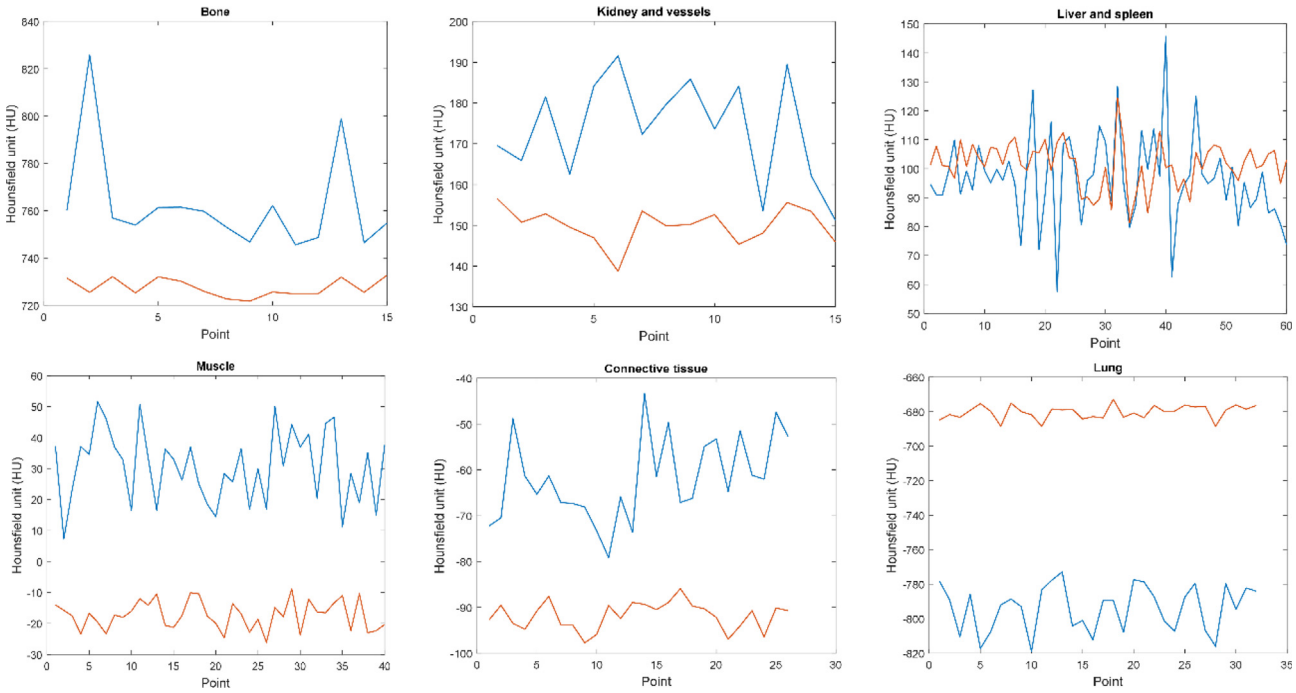

Figure 9. The HU values related to line profiles as indicated in Fig. 3B for the patient scan in comparison to the fabricated anatomical phantom. Blue and red plots represent patient and phantom line profiles, respectively.

and HU results. First, assessing the algorithm behind the gyroid infill pattern generation in Prusa Slicer was not in the scope of this study, even though there may be rounding errors depending on layer thickness and extrusion width in case of small infill percentage increments (like 3–5%) differences specimens. Second, the dosing accuracy of the printing process – expressed as relative weight errors of printed specimens – was in the same order of magnitude as the infill percentage increments which have also likely affected the results. Third, both the printer calibration and the density estimations were using the densities of the printing materials as reported in their technical datasheets, which may slightly deviate from physical reality. Furthermore, the observed nonlinearity behavior can also be related to the achieved standard deviation in reproducibility results. In the case of material 2 and the 91% infill, the reported standard deviation of reproducibility is 32, which is larger than the HU difference between the 91% infill and its immediate neighbors (HU at 91% = 586, HU at 94% = 591, HU at 88% = 604), therefore it may contribute to the nonlinearity pattern of HU values.

We observed lower standard deviation in samples compared to Gammex phantom. The reason may be that for the printed silicone phantoms, the image resolution was lower (coarser) than the resolution of the printed structure (infill structures), so we have the averaged HU and therefore we do not see pixels with unique gray values, resulting in a low standard deviation.

By changing the beam energies, an inverse relationship between the attenuation coefficient and beam hardness was observed for all samples which is typical for bone tissue but is in contrast to soft tissues which exhibit constant HU over different beam energies [36,37]. This indicates a higher effective atomic number of the phantoms compared to water. In addition, for higher infill-densities the increase in HU values with decreasing beam energy was more distinct. Future developments will investigate other types of flexible printable materials/liquids which mimic the attenuation of tissues over a large X-ray energy range. Injection of fluid in the printed structure may also be used to adjust for different radiodensity values. This could be done by either injecting fluid into the infill structure layer-wise during printing or injecting it into the whole phantom manually after printing. Such a strategy is considered as the future perspective of this study. In addition, investigating of the mechanical properties of samples with different infill densities is also a promising future direction of this research. Certain infill structures may provide both matching HUs and matching mechanical properties at the same time for certain tissues. Such cases may be used to create radiologically and mechanically realistic models, which may be especially useful in surgical training or

Please cite this article as: S. Hatamikia, L. Jaksa, G. Kronreif et al., Silicone phantoms fabricated with multi-material extrusion 3D printing technology mimicking imaging properties of soft tissues in CT, Z Med Phys, https://doi.org/10.1016/j.zemedi.2023.05.007

image guided procedures where flexible phantoms are needed.

Data Availability Statement

The code used to extract the data is distributed by the authors as open-source. The patient data can be made available on request due to privacy/ethical restrictions.

Declaration of Competing Interest

The authors declare that they have no known competing financial interests or personal relationships that could have appeared to influence the work reported in this paper.

Acknowledgements

This work has been supported by ACMIT – Austrian Center for Medical Innovation and Technology, which is funded within the scope of the COMET program and funded by Austrian BMVIT and BMWFW and the governments of Lower Austria and Tyrol. This work was also supported by the Provincial Government of Lower Austria (Land Niederösterreich) under grant assignment number WST3-F2- 528983/005-2018.

References

[1] Ligon SC, Liska R, Stampfl J, Gurr M, Mülhaupt R. Polymers for 3D printing and customized additive manufacturing. Chem Rev 2017;117(15):10212–10290. https://doi.org/10.1021/acs.chemrev.7b00074.

[2] Hazelaar C, van Eijnatten M, Dahele M, Wolff J, Forouzanfar T, Slotman B, Verbakel WFAR. Using 3D printing techniques to create an anthropomorphic thorax phantom for medical imaging purposes. Med Phys 2018;45(1):92–100. https://doi.org/10.1002/mp.12644.

[3] Tino R, Yeo A, Leary M, Brandt M, Kron T. A systematic review on 3d-printed imaging and dosimetry phantoms in radiation therapy 1533033819870208. Technol Cancer Res Treat 2019;18. https://doi.org/10.1177/1533033819870208.

[4] Holmes RB, Negus IS, Wiltshire SJ, Thorne GC, Young P. Alzheimer's disease neuroimaging initiative. Creation of an anthropomorphic CT head phantom for verification of image segmentation. Med Phys 2020;47(6):2380–2391. https://doi.org/10.1002/mp.14127.

[5] Kissick LAD et al.. The phantoms of medical and health physics. Med Phys 2016;43(9):5264. https://doi.org/10.1118/1.4960370, PMID: 27587060.

[6] Bieniosek MF, Lee BJ, Levin CS. Technical note: Characterization of custom 3D printed multimodality imaging phantoms. Med Phys 2015;42(10):5913–5918. https://doi.org/10.1118/1.4930803.

[7] Den Otter TD, Schubert J. Hounsfield Unit. 2022 Mar 9. StatPearls, Treasure Island (FL): StatPearls Publishing; 2022, Jan–. PMID: 31613501.

[8] Perrin RL, Zakova M, Peroni M, Bernatowicz K, Bikis C, Knopf AK, Safai S, Fernandez-Carmona P, Tscharner N, Weber DC, Parkel TC, Lomax AJ. An anthropomorphic breathing phantom of the thorax for testing new motion mitigation techniques for pencil beam scanning proton therapy. Phys Med Biol 2017;62(6):2486–2504. https://doi.org/10.1088/1361-6560/62/6/2486.

[9] Mohammed Ali A, Hogg P, Johansen S, England A. Construction and validation of a low cost paediatric pelvis phantom. Eur J Radiol 2018 Nov;108:84–91. https://doi.org/10.1016/j.ejrad.2018.09.015.

[10] McGarry CK, Grattan LJ, Ivory AM, Leek F, Liney GP, Liu Y, Miloro P, Rai R, Robinson AP, Shih AJ, Zeqiri B, Clark CH. Tissue mimicking materials for imaging and therapy phantoms: a review. Phys Med Biol 2020;65(23). https://doi.org/10.1088/1361-6560/abbd17.

[11] Hatamikia S, Oberoi G, Zacher A, Kronreif G, Birkfellner W, Kettenbach J, Ponti S, Lorenz A, Buschmann M, Jaksa L, Irnstorfer N, Unger E. Additively manufactured samples for mimicking soft tissue radiation attenuation in CBCT using Polyjet technology S0939-3889(22)00063-0. Z Med Phys 2022. https://doi.org/10.1016/j.zemedi.2022.05.002.

[12] Hatamikia S, Gulyas I, Birkfellner W, Kronreif G, Unger A, Oberoi G, Lorenz A, Unger E, Kettenbach J, Figl M, Patsch J, Strassl A, Georg D, Renner A. Realistic 3D printed CT imaging tumor phantoms for validation of image processing algorithms. Phys Med 2023;105:102512. https://doi.org/10.1016/j.ejmp.2022.102512.

[13] Filippou V, Tsoumpas C. Recent advances on the development of phantoms using 3D printing for imaging with CT, MRI, PET, SPECT, and ultrasound. Med Phys 2018;45(9):e740–e760. https://doi.org/10.1002/mp.13058.

[14] Ehrbar S, Jöhl A, Kühni M, Meboldt M, Ozkan Elsen E, Tanner C, Goksel O, Klöck S, Unkelbach J, Guckenberger M, Tanadini-Lang S. ELPHA: Dynamically deformable liver phantom for real-time motion-adaptive radiotherapy treatments. Med Phys 2019;46(2):839–850. https://doi.org/10.1002/mp.13359.

[15] Niebuhr NI, Johnen W, Echner G, Runz A, Bach M, Stoll M, Giske K, Greilich S, Pfaffenberger A. The ADAM-pelvis phantom-an anthropomorphic, deformable and multimodal phantom for MRgRT 04NT05. Phys Med Biol 2019;64(4). https://doi.org/10.1088/1361-6560/aafd5f.

[16] de Jong TL, Moelker A, Dankelman J, van den Dobbelsteen JJ. Designing and validating a PVA liver phantom with respiratory motion for needle-based interventions. Int J Comput Assist Radiol Surg 2019;14(12):2177–2186. https://doi.org/10.1007/s11548-019-02029-6.

[17] Higgins M, Leung S, Radacsi N. 3D printing surgical phantoms and their role in the visualization of medical procedures. Ann 3D Print Med 2022;6:100057. https://doi.org/10.1016/j.stlm.2022.100057.

[18] Nhan C, Chankowsky J, Torres C, Boucher LM. Creating low-cost phantoms for needle manipulation training in interventional radiology procedures. Radiographics 2021;41(4):1230–1242. https://doi.org/10.1148/rg.2021200133.

[19] Dimmick S, Jones M, Challen J, Iedema J, Wattuhewa U, Coucher J. CT-guided procedures: evaluation of a phantom system to teach accurate needle placement. Clin Radiol 2007;62(2):166–171. https://doi.org/10.1016/j.crad.2006.09.010.

[20] Gallas RR, Hünemohr N, Runz A, Niebuhr NI, Jäkel O, Greilich S. An anthropomorphic multimodality (CT/MRI) head phantom prototype for end-to-end tests in ion radiotherapy. Z Med Phys 2015;25(4):391–399. https://doi.org/10.1016/j.zemedi.2015.05.003.

[21] Steinmann A, Stafford RJ, Sawakuchi G, Wen Z, Court L, Fuller CD, Followill D. Developing and characterizing MR/CT-visible materials used in QA phantoms for MRgRT systems. Med Phys 2018;45(2):773–782. https://doi.org/10.1002/mp.12700.

[22] Li W, Belmont B, Shih A. Design and manufacture of polyvinyl chloride (PVC) tissue mimicking material for needle insertion. Proc

Please cite this article as: S. Hatamikia, L. Jaksa, G. Kronreif et al., Silicone phantoms fabricated with multi-material extrusion 3D printing technology mimicking imaging properties of soft tissues in CT, Z Med Phys, https://doi.org/10.1016/j.zemedi.2023.05.007

Manuf 2015;1:866–878. https://doi.org/10.1016/j.promfg.2015.09.078.

[23] Liao Y, Wang L, Xu X, Chen H, Chen J, Zhang G, Lei H, Wang R, Zhang S, Gu X, Zhen X, Zhou L. An anthropomorphic abdominal phantom for deformable image registration accuracy validation in adaptive radiation therapy. Med Phys 2017;44(6):2369–2378. https://doi.org/10.1002/mp.12229.

[24] He Y, Qin S, Dyer BA, Zhang H, Zhao L, Chen T, Zheng F, Sun Y, Shi L, Rong Y, Qiu J. Characterizing mechanical and medical imaging properties of polyvinyl chloride-based tissue-mimicking materials. J Appl Clin Med Phys 2019;20(7):176–183. https://doi.org/10.1002/acm2.12661.

[25] Kadoya N, Miyasaka Y, Nakajima Y, Kuroda Y, Ito K, Chiba M, Sato K, Dobashi S, Yamamoto T, Takahashi N, Kubozono M, Takeda K, Jingu K. Evaluation of deformable image registration between external beam radiotherapy and HDR brachytherapy for cervical cancer with a 3D-printed deformable pelvis phantom. Med Phys 2017;44(4):1445–1455. https://doi.org/10.1002/mp.12168.

[26] Talalwa L, Natour G, Bauer A, Drzezga A, Gordji-Nejad A, Beer S. T_1-mapping and dielectric properties evaluation of a 3D printable rubber-elastomeric polymer as tissue mimicking materials for MRI phantoms. Mater Res Express 2020;7:115306.

[27] Talalwa L, Natour G, Bauer A, Drzezga A, Gordji-Nejad A, Beer S. Radiological characteristics of a new experimental rubber elastomeric polymer used in three-dimensional printing with different infill densities and patterns. J Phys Commun 2020;4:125006.

[28] Yeo J, Koh J, Wang F, et al. 3D printing silicone materials and devices. In: Silicon Containing Hybrid Copolymers. Germany: Wiley-VCH Verlag GmbH & Co. KGaA; 2020. p. 239–263.

[29] Coulter F, Schaffner M, Faber J, et al. Bioinspired heart valve prosthesis made by silicone additive manufacturing. Matter 2019;1:266–279. https://doi.org/10.1016/j.matt.2019.05.013 46.

[30] Luis E, Pan HM, Sing SL, et al. Silicone 3D printing: process optimization, product biocompatibility, and reliability of silicone meniscus implants. 3D Print Addit Manufact 2019;6:319–332. https://doi.org/10.1089/3dp.2018.022647.

[31] Luis E, Pan HM, Sing SL, Bajpai R, Song J, Yeong WY. 3D Direct Printing of Silicone Meniscus Implant Using a Novel Heat-Cured Extrusion-Based Printer. Polymers (Basel) 2020;12(5):1031. https://doi.org/10.3390/polym12051031.

[32] Yin J, Dai G, et al. 3D Printed Multi-material Medical Phantoms for Needle-tissue Interaction Modelling of Heterogeneous Structures. J Bionic Eng 2021;18:346–360. https://doi.org/10.1007/s42235-021-0031-1.

[33] Jaksa L, Pahr D, Kronreif G, Lorenz A. Development of a multi-material 3D printer for functional anatomic models. Int J Bioprint 2021 Oct 12;7(4):420. https://doi.org/10.18063/ijb.v7i4.420.

[34] Jaksa L, Pahr D, Kronreif G, Lorenz A. Calibration dependencies and accuracy assessment of a silicone rubber 3D printer. Invent 2022;7:35. https://doi.org/10.3390/inventions7020035.

[35] Hatamikia S, Kronreif G, Unger A, Oberoi G, Jaksa L, Unger E, Koschitz S, Gulyas I, Irnstorfer N, Buschmann M, Kettenbach J, Birkfellner W, Lorenz A. 3D printed patient-specific thorax phantom with realistic heterogenous bone radiopacity using filament printer technology S0939-3889(22)00007-1. Z Med Phys 2022. https://doi.org/10.1016/j.zemedi.2022.02.001.

[36] Dancewicz OL, Sylvander SR, Markwell TS, Crowe SB, Trapp JV. Radiological properties of 3D printed materials in kilovoltage and megavoltage photon beams. Phys Med 2017;38:111–118. https://doi.org/10.1016/j.ejmp.2017.05.051.

[37] Ma X, Figl M, Unger E, Buschmann M, Homolka P. X-ray attenuation of bone, soft and adipose tissue in CT from 70 to 140 kV and comparison with 3D printable additive manufacturing materials. Sci Rep 2022;12(1):14580. https://doi.org/10.1038/s41598-022-18741-4.

[38] Hatamikia S, Oberoi G, Unger E, Kronreif G, Kettenbach J, Buschmann M, Figl M, Knäusl B, Moscato F, Birkfellner W. Additively Manufactured Patient-Specific Anthropomorphic Thorax Phantom With Realistic Radiation Attenuation Properties. Front Bioeng Biotechnol 2020(8):385.

[39] Jaksa L, Aryeetey OJ, Hatamikia S, Nägl K, Buschmann M, Dieter HP, Kronreif G, Lorenz A. 3D-Printed multi-material liver model with simultaneous mechanical and radiological tissue-mimicking features for improved realism. Int J Bioprint 2023 Mar 28;9(4):721. https://doi.org/10.18063/ijb.721.

[40] Oberoi G et al.. 3D printed biomimetic rabbit airway simulation model for nasotracheal intubation training. Front Vet Sci 2020;27(7):587524. https://doi.org/10.3389/fvets.2020.587524.

Please cite this article as: S. Hatamikia, L. Jaksa, G. Kronreif et al., Silicone phantoms fabricated with multi-material extrusion 3D printing technology mimicking imaging properties of soft tissues in CT, Z Med Phys, https://doi.org/10.1016/j.zemedi.2023.05.007